

Interstellar nanodiamonds: the carriers of mid-infrared emission bands?

A.P. Jones and L. d'Hendecourt

Institut d'Astrophysique Spatiale (CNRS), Université Paris XI – Bâtiment 121, 91405 Orsay Cedex, France

Received 7 September 1999 / Accepted 21 December 1999

Abstract. In this paper we pursue the natural consequences of the structure of nanodiamonds and their surface relaxation and reconstruction to surfaces exhibiting sp^2 carbon atoms. We show that in the interstellar radiation field nanodiamonds can be stochastically heated to temperatures as high as 1000 K and give rise to discrete emission bands associated with the surface structures. We therefore speculate that nanodiamonds can make a significant contribution towards the 3 – 15 μm unidentified mid-infrared emission bands.

Key words: ISM: dust, extinction – ISM: general

1. Introduction

Diamonds were first proposed as a component of interstellar dust by Saslaw & Gaustad in 1969. However, it was only in 1987 that presolar nanometre-sized diamond grains (nanodiamonds) were first detected, not in the interstellar medium, but in the extracted fractions from primitive meteorites (Lewis et al. 1987). These diamond grains are composed of almost pure carbon with less than 1% by mass of impurities with atomic masses greater than 6 (Bernatowicz et al. 1989). They contain isotopic anomalies, e.g., ^{15}N depletions and likely p - and r -process Xe compositions, and enhanced D/H ratios, that clearly indicate a presolar origin (e.g., Anders & Zinner 1993).

Nanodiamonds are, by over two orders of magnitude in mass, the most abundant presolar grains recovered from primitive meteorites. Their euhedral morphologies (well-formed crystal shapes) indicate that they have undergone little alteration (Daulton et al. 1996).

It has been postulated that interstellar diamonds will be observable only with great difficulty (Lewis et al. 1989). This is, however, a conclusion inferred principally from the extrapolation of the bulk diamond properties to nanometre size-scales. However, as Bernatowicz et al. (1989) caution, attempting to model interstellar diamonds as smaller versions of macroscopic diamond will lead to errors.

The search for observable intrinsic nanodiamond properties in the laboratory has been hampered by their high surface to

volume ratio and active surface chemistry (Hill et al. 1998). The infrared spectra of the extracted nanodiamonds are dominated by surface adsorbates introduced during laboratory extraction and, as Hill et al. (1998) pointed out, this is clearly the case with many published presolar nanodiamond spectra (e.g., Koike et al. 1995; Mutschke et al. 1995; Andersen et al. 1998). This active surface chemistry, while aiding their extraction (e.g., Anders & Zinner 1993), has clearly been a hindrance to the search for observable nanodiamond signatures.

Allamandola et al. (1992, 1993) suggested that an absorption band at 3.47 μm could be due to a tertiary carbon CH stretching mode on the surfaces of nanodiamonds. However, this band is probably not unique to nanodiamonds as it seems that it could have other origins (Brooke et al. 1996). Recently, Guillois et al. (1999) showed that infrared emission features observed at 3.43 and 3.53 μm in two sources are well-matched by surface CH groups on ~ 50 nm radius diamond particles.

Lewis et al. (1989) suggested that diamond grains may be detectable in emission, and Hill et al. (1998) noted that they may only be observable in emission. Hill et al. (1998) showed that a diamond feature at ~ 21 μm was consistent with the unidentified emission feature seen at this wavelength in some carbon-rich protoplanetary nebulae (PPNe).

The measurement of the intrinsic infrared to ultraviolet spectra of nanometre-sized diamond particles and their physical properties is central to determining the observability of interstellar nanodiamonds. The extrapolation of bulk diamond properties is clearly not appropriate because a large fraction of the atoms are in or near the surface where the structure is different from that of the bulk material. In this paper we model the structural properties of nanometre-sized diamonds and discuss their infrared properties.

2. The formation of nanodiamonds

Presolar nanodiamonds were originally isolated on the basis of their anomalous Xenon isotopic ratios, the so-called Xe-HL meteoritic component (Lewis et al. 1987). This isotopic component seems to indicate a supernova origin for the nanodiamonds. However, their formation in supernovae is seemingly inconsistent with the requirement for a carbon-rich environment (e.g., Lewis et al. 1989).

Daulton et al. (1996) showed that the twinning structures and the paucity of dislocations within the bulk structure of meteoritic nanodiamonds imply rapid, isotropic growth and vapour phase processes for their formation. The measured Log-normal nanodiamond size distribution also seems to be consistent with a growth mechanism rather than a fragmentation formation process, and indicates minimal contribution from sputtering and erosion processes (Lewis et al. 1989; Daulton et al. 1996).

In the chemical vapour deposition (CVD) formation of diamond in the laboratory, growth occurs at the gas-solid interface and both atomic hydrogen and oxygen play important roles in the preferential erosion of non-diamond carbon, principally graphitic carbon, from the growth surface (e.g., Angus et al. 1989). The synthesis of diamond in the laboratory requires $0.8 \leq C/O \leq 1.3$ (Bachmann et al. 1991) which is entirely consistent with the observed C/O ratios for carbon stars (Lambert et al. 1986).

Although diamond growth by CVD processes is now reasonably well understood (e.g., Angus et al. 1989), the initial nucleation process is not clear. It is, however, clear that the graphite/diamond interface plays a very fundamental role in CVD diamond formation and growth (e.g., Lambrecht et al. 1993). Lambrecht et al. (1993) have shown that the initial formation steps in diamond growth can occur by nucleation on a graphite surface through a hydrogenation process. Interestingly, C₆₀ and C₇₀ fullerenes have also been shown to act as diamond nucleation centres under CVD conditions and to induce high diamond nucleation rates (Meilunas et al. 1991). These very fundamental processes therefore point towards a very intimate connection between sp³ diamond and sp² graphite surfaces and interfaces.

Nanodiamonds can also be formed by the intense ultraviolet irradiation of graphitic and amorphous carbon particles (Fedoseev et al. 1983; Alam et al. 1989). Such processes in the astrophysical context have been invoked to explain diamond formation in supernovae (Nuth & Allen 1992; Ozima & Mochizuki 1993). However, the thermal processing of nanodiamonds at temperatures of the order of 1400–1800 K leads to the loss of the diamond structure and their conversion to onion-like graphitic particles (Kuznetsov et al. 1994). It has been noted that, at relatively low temperature, pressure exerted on graphite along the direction of the crystallographic *c*-axis can induce the formation of lonsdaleite (see discussion of diamond polytypes by Daulton et al. 1996). The presence of lonsdaleite in meteorites may therefore indicate the shock transformation of graphite in the interstellar medium (e.g., Tielens et al. 1987). However, this diamond polytype can also have a low-pressure origin (Frenklach et al. 1989) and so the evidence for shock-produced interstellar nanodiamonds is equivocal. The contribution of shock-produced nanodiamonds to the meteoritic nanodiamond budget seems, in any event, to be small (Daulton et al. 1996).

3. Presolar nanodiamonds: Structure, size and shape

The cubic form of diamond has a structure consisting of two interleaved face-centred cubic (fcc) lattices, but diamond also

has a hexagonal structural form (lonsdaleite) which is thought to be the less stable of the two. The presolar nanodiamonds clearly show the characteristics expected of the perfect cubic diamond fcc lattice (e.g., Bernatowicz et al. 1990; Daulton et al. 1996). However, it has long been known that perfect diamond (111) surfaces can reconstruct to (2×1) and/or (2×2) sp²-dominated structures (e.g., Vanderbilt & Louie 1984; Mitsuda et al. 1991).

In several studies (Blake et al. 1988; Bernatowicz et al. 1990; Dorschner et al. 1996; Hill 1998) an observed $1s \rightarrow \pi^*$ transition in the electron energy loss spectra (EELS) of meteoritic nanodiamonds was taken to be evidence for the presence of a π -bonded carbon component on the surfaces. The observation of this intimately related sp² component in these studies was taken to be strong evidence for surface reconstruction in nanometre-sized diamonds and was assumed to be a natural consequence of the small particle sizes. The corresponding sp²/sp³ ratios were found to be $\sim 25\%$ (Blake et al. 1988), $> 25\%$ (Bernatowicz et al. 1990), $\sim 20 - 27\%$ (Dorschner et al. 1996) and $\sim 10 - 20\%$ (Hill 1998).

Bernatowicz et al. (1990) found that the surface material most consistent with their EELS data was a form of hydrogenated amorphous carbon (a-C:H), rather than graphite or amorphous carbon (a-C). In particular, they noted the constancy of the proportion of π -bonded carbon (sp²) to fcc carbon (sp³) in the meteoritic nanodiamonds. They modelled their EELS spectra using diamond mantled with graphite, a-C and a-C:H, and found a best fit for 46% by volume of fcc diamond and 54% by volume of a-C:H (with 35 – 60% of hydrogen) which was assumed to be in the form of a coating on the presolar diamonds. These data are consistent with the fact that the nanodiamond residues are brown and transparent, i.e., neither black, as expected for graphite and a-C, nor completely transparent, as would be the case for pure uncoated diamond. In addition, they found that the specific density of the nanodiamonds (2.22–2.33 g cm⁻³, Lewis et al. 1987) was entirely consistent with this two component diamond core and a-C:H coating.

Daulton et al. (1996) have shown that the shape of the presolar nanodiamonds is variable but that well-faceted particles (euhedral morphologies) predominate. For the examined meteoritic nanodiamonds they find significant departures from spherical geometry, Log-normal size distributions and a median radius of ~ 1.4 nm.

4. A model for the structural properties of nanometre-sized diamonds

The fraction of surface and near surface carbon atoms in a nanometre-sized diamond particle will be only weakly dependent upon the particle size. This is simply because the number of surface atoms varies as the square of the particle radius while the total number of atoms varies as the cube of the radius. The ratio of the number of surface atoms to the total number of atoms is then simply proportional to the inverse of the particle radius. Thus, a factor of eight increase in the nanodiamond mass (or a doubling of the radius) will lead to only a factor of two decrease in the fraction of surface atoms. For the $\sim 1 - 2$ nm radius

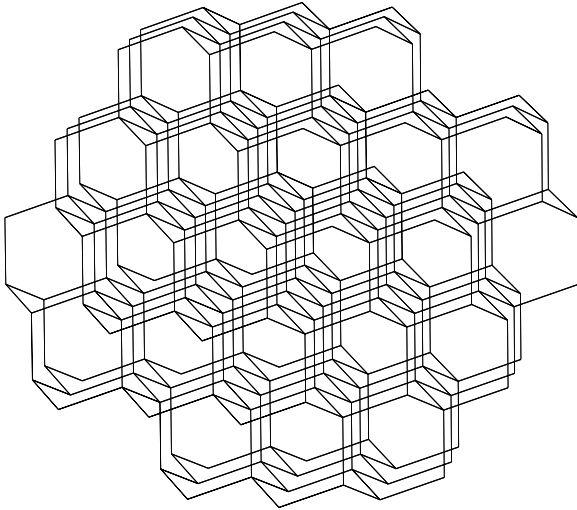


Fig. 1. A 226 carbon atom diamond nanoparticle. In this stick figure of the three-dimensional particle the end-points of each line, which represents a C–C bond, mark the position of a carbon atom in the fcc diamond lattice. The upper, lower, upper right and lower left faces are predominantly diamond (111)-type crystal planes. The upper left and lower right are predominantly diamond (100)-type crystal planes. The front and back faces are composed of (111)-type and (100)-type crystal planes (as per the left and right faces seen edge-on).

presolar diamonds the surface atom fraction thus only varies by a small factor. For the measured meteoritic nanodiamonds the size distribution seems to be relatively independent of the source meteorite (e.g., Bernatowicz et al. 1990; Daulton et al. 1996) and so the surface atom fraction for presolar diamonds is essentially constant.

We have computed the structural properties of approximately spherical nanodiamond particles using a cubic grid filled with sp^3 carbon atoms according to the cubic fcc diamond structure. We then generated a nanodiamond particle by selecting only those carbon atoms within a defined radius. In order to model compact structures we remove from the particle any carbon atoms that are only attached to one other carbon atom (the primary, 1° , carbon atom sites). As a result the particles exhibit spheroidal shapes showing some reasonably well-defined diamond (111)-type and (100)-type crystallographic faces. In Fig. 1 we show an example of a 226 carbon atom diamond particle of radius ≈ 0.6 nm. The illustrated particle exhibits (111)-type and (100)-type crystallographic faces which contain approximately equal numbers of carbon atoms. Although, as we show below the (111)-type faces are more abundant in these particles.

In Table 1 we show the results for nanodiamond structures with radii in the $\approx 0.6 - 2.1$ nm range which covers the typical presolar nanodiamond sizes ($\sim 1 - 2$ nm). The data in Table 1 show the number of secondary, 2° , tertiary, 3° , and quaternary, 4° , (bonded to 2, 3 and 4 other atoms, respectively), sp^3 carbon atoms as a function of the particle size. Within these structures only atoms bonded to four others (4° atom sites) can be within the bulk, and those bonded to less than four (2° and 3° atom sites) must be surface atoms in the absence of internal

Table 1. Model results for typical meteoritic nanodiamond-sized structures. The right hand column gives the ratio of the number of surface atoms to the total number of carbon atoms in the particle.

\approx Radius (nm)	Number of sp^3 carbon atoms				Fraction in surface
	Total	2°	3°	4°	
0.6	226	42	60	124	0.45
1.0	678	78	140	460	0.32
1.2	1274	120	218	936	0.27
1.4	2124	180	304	1640	0.23
1.7	3275	225	436	2614	0.20
1.9	4851	270	584	3997	0.18
2.1	6728	336	740	5652	0.16

vacancies. The surface to total carbon atom ratio is then simply the number of 2° and 3° atoms divided by the total number of atoms. We also note that the (111)-type faces contain only 3° carbon atoms and that the (100)-type faces contain only 2° carbon atoms (Fig. 1). From the total number of 2° and 3° carbon atoms in the particles (Table 1) we therefore conclude that in these particles there are approximately twice as many atoms in the (111)-type crystallographic face structures as in the (100)-type faces. This preference may be further accentuated in the meteoritic diamonds which show euhedral morphologies and significant departures from spherical shapes.

Obviously the dangling bonds on the surfaces of these small diamond particles (due to carbon atoms bonded to less than four others) can be terminated with hydrogen atoms. If this is the case then on the grain surface we will find only sp^3 CH_2 (2°) and CH (3°) groups. Recall that we have deliberately excluded primary, 1° , carbon atoms and hence there can be no CH_3 groups on the generated particles. The surface hydrocarbon groups are generally isolated from one another by at least one carbon atom of higher order on the regular crystal faces, i.e., 2° CH_2 groups are separated by 3° and 4° sites, and 3° CH groups are separated by 4° sites. However, along the particle edges this is no longer true because many adjacent carbon atoms are hydrogenated.

The formulae for the diamond particles in Table 1 are then; $C_{226}H_{144}$, $C_{678}H_{296}$, $C_{1274}H_{458}$, $C_{2124}H_{664}$, $C_{3275}H_{886}$, $C_{4851}H_{1124}$ and $C_{6728}H_{1412}$. The H/C ratios lie between 0.64 for the smallest particles and 0.21 for the largest. In Fig. 2 we show the structure of the perfect fcc nanodiamond particle of radius ≈ 1.4 nm (Table 1). This particle corresponds to approximately the mean meteoritic diamond dimensions (Daulton et al. 1996).

The discussion, so far, has considered only the case of the perfect fcc diamond lattice terminated with sp^3 CH bonds. However, the evidence presented in Sect. 3 clearly shows that diamond surfaces can reconstruct to structures that are dominated by sp^2 carbon atoms. It is thus necessary to consider the consequences for this surface reconstruction in the above structural model. In the absence of overlying layers of a different carbon composition, which we consider below, a limit to the effects of surface reconstruction can be estimated by assuming that all surface 2° and 3° atom sites become sp^2 carbon atom sites. In this hypothetical sp^2 limit we can assume that all surface CC bonds

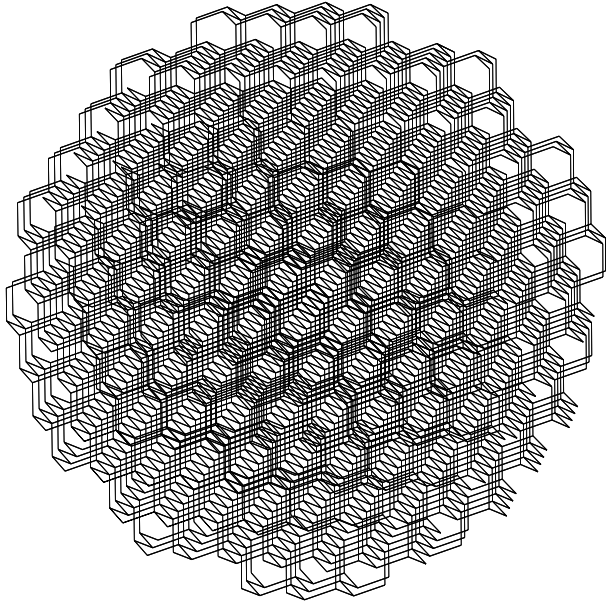


Fig. 2. An idealised spheroidal meteoritic diamond nanoparticle with perfect fcc structure and radius ≈ 1.4 nm. Again, in this stick figure of the three-dimensional particle the end-points of each line, which represents a C–C bond, mark the position of a carbon atom in the fcc diamond lattice. In the profile of this particle it can be seen that the upper, lower, upper right and lower left faces are dominated diamond (111)-type crystal planes, and the upper left and lower right are diamond (100)-type crystal planes.

are entirely olefinic or aromatic and identical in character, and that this results from the breaking of the bonds between 3° sites only. In Fig. 3 we show a schematic cross section of the reconstructed surface of a nanodiamond. As Figs. 1, 2 and 3 show, the reconstruction of the surface to sp^2 will result in the majority of the surface olefinic or aromatic CH bonds having solo and duo CH configurations with perhaps some trio CH groups present at steps and edges on the surface. The fraction of the duo and trio sites may diminish somewhat as the particle size increases, but the solo/(duo+trio) CH ratio will not be particularly sensitive to the particle size. It is intriguing to note that about half of the surface CH bonds could be solo (see Fig. 3) and that this is relatively independent of the particle size.

Bernatowicz et al. (1990) find that a surface layer of a-C:H with about an equal volume to the diamond grain centre is consistent with their EELS data. This implies that on average the a-C:H layer has a thickness of about 0.3 times the radius of the diamond core (as schematically shown in Fig. 3). For a 0.6 nm radius grain, such as the one shown in Fig. 1, this is equivalent to about one monolayer of a-C:H or the complete reconstruction to the sp^2 configuration of all the surface C–C bonds in this particle. For the more typical meteoritic diamond dimensions (radius ~ 1.4 nm, e.g., Fig. 2) this would correspond to 2–3 monolayers of a-C:H, or equivalently the outer 2–3 atomic layers existing in a reconstructed sp^2 configuration (e.g., Fig. 3).

The model presented here rests principally upon the hypothesis that the surfaces of interstellar nanodiamonds will recon-

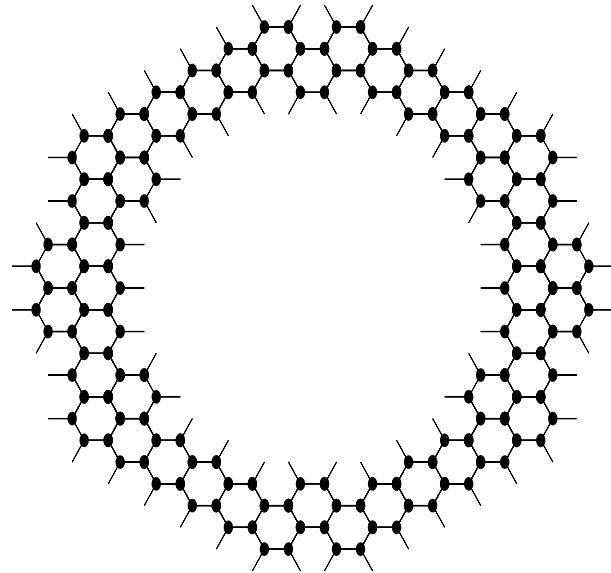


Fig. 3. Schematic cross section of the reconstructed sp^2 surface layer of a ~ 1.5 nm radius nanodiamond particle with an ellipticity of 0.95 typical of the meteoritic nanodiamonds (Daulton et al. 1996). This structure is analogous to the periphery of a large compact PAH structure. The filled circles represent surface and near-surface sp^2 carbon atoms, and the lines between them represent C–C bonds. The lines pointing inward represent connections to the core diamond structure. Each line pointing outward represents a surface CH bond. In this schematic section through the nanoparticle it can be seen that there are only solo and duo CH groups present in about equal numbers.

struct to an sp^2 hydrogenated configuration. The reconstruction process seems in little doubt (e.g., Blake et al. 1988; Bernatowicz et al. 1990; Mitsuda et al. 1991; Chin et al. 1992; Dorschner et al. 1996; Hill 1998), however, the role of hydrogen on these nanodiamond surfaces is not yet clear. On macroscopic diamond crystal faces this surface reconstruction can be transformed back to a sp^3 dominated surface by hydrogen atom adsorption (e.g., Chin et al. 1992). Whether or not this same process can occur on a nanodiamond particle in the interstellar medium is not at all clear. Although, the presence of meteoritic presolar diamonds with a considerable sp^2 surface component (Bernatowicz et al. 1990) would seem to indicate strongly that the surface reconstruction is preserved in nanometre-sized diamonds.

5. The infrared properties of nanodiamonds

With the above assumption that the outer few layers of the presolar nanodiamonds are reconstructed to a sp^2 state from their usual sp^3 hybridisation state, we can make some important deductions on the infrared properties of nanodiamonds. Here we assume that sp^3 surface atoms reconstruct to sp^2 carbon atoms and that all dangling carbon bonds are hydrogenated. We now consider the contributions that nanodiamonds can make to the observed infrared emission from interstellar dust.

One somewhat intriguing aspect of the observed and unidentified interstellar and circumstellar infrared emission bands in the 3–15 μm wavelength region is the approximate con-

stancy of the band positions, widths and the band-to-band intensity ratios in the most common types of infrared emission band spectra (e.g., Geballe 1997, Boulanger 1999). This seems to imply that the carriers of these bands show little variation in their composition from one region to another, and over five orders of magnitude in the radiation field intensity (Boulanger 1999). Aromatic hydrocarbon materials (Duley & Williams 1983) and polycyclic aromatic carbons, PAHs, (Léger & Puget 1984) were long ago proposed as the carriers of the unidentified infrared emission bands. It has always been somewhat difficult to explain the apparent constancy and the band widths and positions with the PAH hypothesis because of the widely varying spectral characteristics exhibited by these large planar molecular species. However, recent attempts at matching the emission band spectrum of several sources (Allamandola et al. 1999) have been more successful. A coal model for the origin of the emission bands (Papoular et al. 1989) was also proposed and has provided a good match to the observed emission band positions and profiles. However, this model too is not without its problems regarding, in particular, the emission mechanism (e.g., Puget et al. 1995).

One solution to the conundrum of the uniformity of the emission bands would be to put the PAH-type of emitting species on the surface of a three-dimensional particle, which would then greatly reduce variations in the carrier structures and hence the variability of their emission spectra. Small grains of non-carbonaceous materials, e.g., silicates or metal oxides, will not provide the correct lattice structure for the preservation of the planar sp^2 carbon atom surface-coating structures. Thus, nanodiamond surfaces appear to be the only viable species with the ability to preserve planar sp^2 carbon atom surface structures on a resilient particle.

5.1. Bulk features

Quaternary (4°) sp^3 carbon atoms in the bulk of a perfect diamond lattice probably play little role in the observable properties of nanodiamonds; other than contributing to the overall particle size and absorption at ultraviolet wavelengths. However, defects within the bulk due to vacancies or substituted nitrogen atoms could be responsible for emission features in the $7 - 30 \mu\text{m}$ region. Defects break the lattice symmetry and allow one phonon modes to become active in this wavelength region. In the perfect diamond lattice only two and three phonon modes are allowed (e.g., Hill et al. 1998; Hill 1998). Two and three phonon modes in the $3.5 - 5.5 \mu\text{m}$ region are suppressed in nanodiamonds and will be very weak with respect to surfaces modes and CC and CH features (Hill 1998). Infrared-active modes in the $6 - 15 \mu\text{m}$ region in defective diamonds (Morelli et al. 1993; Hill et al. 1998) may be equivalent to the $6 - 15 \mu\text{m}$ infrared modes expected from nanodiamond surface structures. However, these will be surface and not bulk features. As an example of the importance of bulk modes in interstellar nanodiamond particles Hill et al. (1998) have shown that a band at $\sim 21 \mu\text{m}$ in defective diamonds may be related to the observed $\sim 21 \mu\text{m}$ emission band observed in some carbon-rich PPNe.

Defects, such as vacancies and nitrogen atoms, also exist within the bulk structure of nanodiamonds. Hill et al. (1997) pointed out that the anomalous nitrogen component in the meteoritic diamonds is only liberated at high temperatures in combustion experiments. This nitrogen must therefore be embedded within the crystallite structure.

In the meteoritic nanodiamonds the nitrogen atom concentration is at most 13,000 ppm (Russell et al. 1996). As Hill et al. (1997) showed this is equivalent to only one nitrogen atom in a 1 nm radius nanodiamond and of the order of $1 - 10$ nitrogen atoms in a 2 nm particle. Thus, there are few nitrogen atoms per nanodiamond but their signatures may still be detectable. They will be very weak in absorption and probably only detectable in emission. Interestingly, the nitrogen impurities in the diamond lattice show infrared absorption bands in the $7 - 10 \mu\text{m}$ region. In particular, bands at 8.8, 7.8 and $8.6 \mu\text{m}$ due, respectively, to one, two, and four nitrogen atom substitutions for carbon in the diamond lattice are seen (e.g., Davies 1977). Braatz et al. (1998) argue, based on their presolar diamond spectra, that the 8.6 and $8.8 \mu\text{m}$ bands are probably the most likely bands in presolar diamonds.

5.2. Surface features

The infrared spectroscopy of presolar nanodiamonds has shown that surface species dominate the measured spectra, as Hill et al. (1998) demonstrated. The strongest nanodiamonds modes will therefore be those associated with surface groups and structures. Following the conclusion of Bernatowicz et al. (1990), that the surface layer of the presolar diamonds appears to be similar to an a-C:H material, we adopt a-C:H as a model for the nanodiamond surface structure. We then take the infrared signatures of a-C:H materials (e.g., Robertson 1986) as an indicator of the infrared properties of reconstructed nanodiamond surfaces: see next subsection and the discussions in Sect. 4. It is clear that aromatic or olefinic CH and CC modes should dominate and could be observable as a set of infrared emission bands from particles heated by the the interstellar radiation field provided that they can reach an appropriate emission temperature (see Sect. 6).

Solo and duo CH modes will dominate because many of the surface CH groups will be isolated. Trio CH groups may also be present at the particle edges but will be much less abundant than the solo and duo CH groups. As noted in Sect. 4 and by Bernatowicz et al. (1990) the surface composition of nanodiamonds is relatively independent of the particle size. Therefore the infrared emission bands and the band-to-band intensity ratios should be relatively insensitive to the particle size.

5.3. The infrared modes of nanodiamonds

The reconstructed surfaces of nanodiamonds may be very closely related to the diamond-like a-C:H materials (Bernatowicz et al. 1990) that have been extensively studied in the laboratory (e.g., Angus et al. 1989). Thus, based on the interpretation of the infrared features seen in laboratory a-C:H materials (e.g., Robertson 1986) we present in Table 2 some of the expected

Table 2. The expected infrared modes of surface-reconstructed nanodiamond a-C:H surfaces (Bernatowicz et al. 1990) based on the laboratory data for a-C:H (Robertson 1986), with the exception of the 8.6 μm band assignment which was taken from Allamandola (1989). Relative band strengths have not been assigned.

Band Position		Origin of the Band
μm	cm^{-1}	
C—H stretching modes		
3.28	3045	sp^2 aromatic C—H
3.33	3000	sp^2 olefinic C—H
3.42	2920	sp^3 CH & CH ₂
3.51	2850	sp^3 CH ₂
C—H bending modes		
8.6	1150	sp^2 aromatic, in-plane
11.36	880	sp^2 solo aromatic, out-of-plane
12.2–12.8	780–820	sp^2 duo/trio aromatic, out-of-plane
C—C modes		
6.17	1620	sp^2 olefinic C—C stretch
6.37	1570	sp^2 aromatic C—C stretch
6.63	1509	?
6.99	1430	sp^2 aromatic C—C stretch
7.32	1367	disorder mode
7.69	1300	sp^3 C—C stretch

infrared active modes for surface-reconstructed nanodiamonds. The reconstruction or aromatisation of a nanodiamond surface and the formation of sp^2 carbon atom CC and CH bonds requires a suppression of sp^3 surface carbons. If this process is incomplete the residual sp^3 CH bonds will give rise to aliphatic 3.4 and 3.5 μm CH features. Hill (1998) has shown that the ~ 3.42 and ~ 3.53 μm bands of the diamond precursor molecule adamantane, $\text{C}_{10}\text{H}_{16}$, may be consistent with the observed emission bands at these wavelengths in some PPNe, and Guillois et al. (1999) have shown them to be consistent with ~ 50 nm radius diamond particles.

The tabulated feature assignments given by Robertson (1986) do not include a band at ~ 8.6 μm . However, the infrared absorption spectra presented do show some structure on the long wavelength side of the band centred at ~ 8 μm which could be related to a feature at ~ 8.6 μm seen in the interstellar medium (e.g., Allamandola 1989). The infrared bands seen in laboratory a-C:Hs (Table 2) thus bear a remarkable wavelength coincidence to the strong infrared emission bands observed at 3.3, 6.2, 7.7, 8.6, 11.3 and 12.7 μm and also to the weaker bands at 3.4 and 3.51 μm (e.g., Allamandola 1989). Kapitonov & Kon'kov (1998) noted this similarity in the a-C:H bands and proposed these materials as carriers of the unidentified mid-infrared emission bands. Similarly, Koike et al. (1995) suggested that diamond-like materials could be one of the carriers of the minor unidentified infrared bands.

The most commonly observed emission spectra show dominant bands at 3.3, 6.2, 7.7 and 11.3 μm , weaker bands at 3.4, 5.25 and 8.6 μm , and broad plateaux in the 3.3 – 3.6 and 11.3 – 12.6 μm regions (Geballe 1997). In addition a weak

band at 11.0 μm also seems to be a common feature of these spectra (e.g., Verstraete et al. 1996). Without detailed modelling of the of the surface bonds on nanodiamonds it is clearly premature to attempt to explain all of the commonly observed emission bands in terms of the emission from these grains. We do, however, note one interesting fact that may be of relevance, concerning the position of the solo CH band in the linear PAHs anthracene, tetracene and pentacene. As the laboratory infrared spectral catalogues (e.g., Aldrich and Sadtler) show, for this series of PAHs, the solo CH band occurs at 11.3, 11.1 and 11.0 μm for the three, four and five adjacent rings, respectively. For the non-linear three to five ring PAHs the catalogues show that the solo CH band always occurs in the 11.2 – 11.5 μm region. Thus, it appears that as the number of unperturbed adjacent solo CH sites increases the 11 μm band shifts to shorter wavelengths. Such a linear arrangement of solo CH groups is analogous to the structures expected to form on nanodiamond surfaces (see Sect. 4 and Fig. 3). Conversely, in the non-linear PAHs the solo CH sites are usually not adjacent, and are often perturbed by steric effects due to the location of adjacent CH groups at concavities at the edge of the PAHs. These sites would be analogous to the CH groups at, and near, steps and edges on a nanodiamond surface. Thus, as a natural consequence of the surface structure of nanodiamond particles, the presence of a weak band at 11.0 μm and the origin of the more prominent 11.3 μm band can be explained.

6. The thermal properties of nanodiamonds

The meteoritic nanodiamonds provide a model for the properties of the stochastically-heated interstellar grains with sizes intermediate between PAH molecules and large grains, i.e., the so-called Very Small Grains (VSGs, Désert et al. 1990). The presolar nanodiamonds are, in effect, core/mantle particles with cores that absorb strongly at ultraviolet wavelengths, and mantles that emit at infrared wavelengths. Thus, because the heat capacity per unit volume of diamond is greater than that of graphite and a-C:H, and because diamond is a weak infrared emitter, the diamond core will act as a thermal reservoir that pumps infrared emission from the surface material.

We have estimated the thermal properties of the meteoritic diamonds in order to calculate the maximum temperatures of these particles upon absorption of a single photon from the interstellar radiation field. In this calculation we assumed the nanodiamond structure of Bernatowicz et al. (1990), i.e., 46% by volume of fcc diamond and 54% by volume of a-C:H in the form of a coating. For the diamond heat capacity we used the data from Lide (1992) and adopted a Debye temperature, θ , of 2034.4 K to extrapolate these data to lower temperatures using $C(T)_d \propto (T/\theta)^3$ smoothly fitted to the Lide (1992) data at 300 K. As we do not know the heat capacity of the a-C:H coating material we have adopted the heat capacity for graphite from Lide (1992) and extrapolated this to lower temperatures using a Debye temperature of 1819.7 K, in the same way as for the diamond core. However, in this case we make allowance for the lower density of a-C:H, with respect to graphite, by multiplying

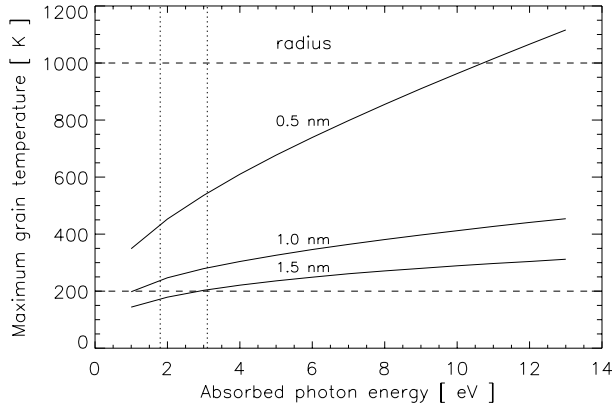


Fig. 4. Nanodiamond maximum temperatures as a function of particle size and absorbed photon energy. The horizontal dashed lines mark the approximate range of dust temperatures required to produce the infrared emission bands (~ 200 to 1000 K). The vertical dotted lines mark the visible photon energy range.

the derived heat capacity by the ratio of the specific densities, (ρ_a/ρ_g) , where ρ_a and ρ_g are the specific mass densities of a-C:H and graphite, respectively. We also make allowance for the fact that the particle surface is hydrogenated and that these hydrogen atoms can contribute to the heat capacity. For the CH bond heat capacity, $C_H(T)$, we use the values given by Dwek et al. (1997). The specific heat capacity of a nanodiamond particle, as a function of its radius a , can therefore be estimated using the following expression,

$$C(T) = \left[0.46 N(a)_d C_C(T)_d + 0.54 N(a)_a (\rho_a/\rho_g) C_C(T)_g + N_{sH}(a)_a C_H(T) \right] / \frac{4}{3}\pi a^3, \quad (1)$$

where, $N(a)_d$ and $N(a)_a$ are the number of atoms in the diamond and a-C:H phases and $C_C(T)_d$ and $C_C(T)_g$ are the heat capacities per carbon atom for diamond and graphite, respectively. $N_{sH}(a)_a$ is the number of surface hydrogen atoms on the a-C:H mantle (we have assumed 50% surface coverage in our calculations).

In Fig. 4 we show the maximum nanodiamond temperature, T_{max} , as a function of the particle size and the absorbed photon energy, E , calculated by solution of the equation,

$$E = \frac{4}{3}\pi a^3 \int_{T_0}^{T_{max}} C(T) dT, \quad (2)$$

where, T_0 is the grain temperature prior to photon absorption which we have taken to be zero. For grains to emit efficiently at wavelengths in the $3 - 15 \mu\text{m}$ region they must have temperatures in the range $200 - 1000$ K. From Fig. 4 we can see that emission in the $3 - 15 \mu\text{m}$ region from nanodiamond surface sp^2 CC and CH groups requires grain radii in the $0.5 - 1.5$ nm range, i.e., sizes entirely consistent with the presolar meteoritic diamonds.

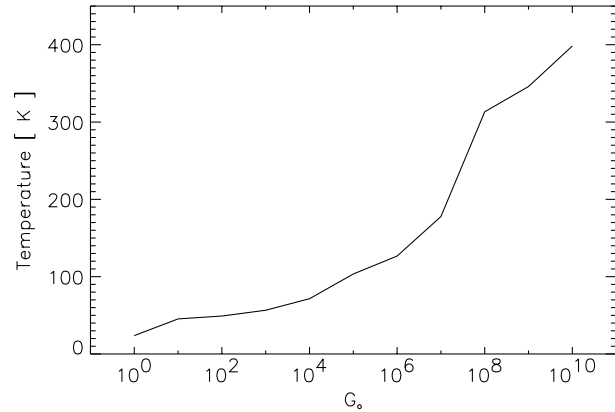


Fig. 5. Nanodiamond equilibrium temperatures as a function of the intensity of the interstellar radiation field, in units of the standard local radiation field in the Solar neighbourhood, G_0 . In this regime, particle size \ll wavelength, the nanodiamond temperatures are independent of the radius.

We therefore find that small interstellar nanodiamonds, with radii of the order of 0.5 nm, will likely have maximum temperatures of the order of 1000 K for ultraviolet photon absorption. Such high temperatures are likely to eject loosely bound surface species and thus continually scrub the grain surfaces clean of weakly adsorbed atoms or molecular groups. This process may therefore provide the means to preserve the surface structure and composition of the interstellar nanodiamonds.

In Fig. 5 we show the equilibrium temperatures of nanodiamonds as a function of the radiation field in units of G_0 , where G_0 is the radiation field in the Solar neighbourhood. The data in Fig. 5 were calculated using Q_{abs} values in the long wavelength limit derived for core/mantle grains using the a-C:H refractive index data (sample BE of Rouleau & Martin 1991) and the diamond refractive index data from Roberts & Walker (1967). Note that in Fig. 5 the nanodiamond equilibrium temperatures are much less than the maximum temperatures shown in Fig. 4. Stochastic heating will therefore be the dominant heating process for nanodiamonds in almost all radiation field environments. However, if the calculated equilibrium temperatures, for $G_0 < 10^4$ (i.e., $\sim 25 - 70$ K), are indicative of the mean nanodiamond temperatures, then this implies continuum emission from these grains in the $\sim 40 - 120 \mu\text{m}$ region.

Infrared continuum emission from nanodiamonds will probably be sensitive to the thermal connectivity between the bulk atoms and the surface structures. In low excitation regions emission from the surface CC and CH modes will dominate in the mid-infrared because the grain thermal energy will be channelled through these modes. In high excitation regions the bulk may also contribute to the emission at the same time as continuing to pump the surface emission modes. Thus, at higher grain temperatures the bulk infrared bands in the diamond one phonon region, i.e., in the $10 - 15$ and $\sim 21 \mu\text{m}$ bands, may also be seen in emission (Hill et al. 1998). The diamond two and three phonon nanodiamond modes in the $3.5 - 5.5 \mu\text{m}$ region may also appear as two weak emission bands centred at $\sim 4 \mu\text{m}$

and $\sim 5 \mu\text{m}$ (Hill 1998). Interstellar nanodiamonds heated to temperatures of the order of 1000 K (Fig. 4) may also be responsible for continuum emission at wavelengths of the order of a few microns.

The grain temperature arguments presented here are consistent with emission features in the mid-infrared from surface CC and CH groups on nanodiamond surfaces. However, because of uncertainties in the details of the calculation of the specific heat capacities of nanometre-sized amorphous particles these conclusions need to be verified experimentally. Clearly, in order for nanodiamonds to be responsible for the mid-infrared emission bands their sizes must extend down to sizes of 0.5 nm. In the log-normal size distribution of the presolar diamonds in the Murchison meteorite particles with radii smaller than 0.5 nm seem to be present (Daulton et al. 1996). The presolar diamond size distribution therefore seems to be entirely consistent with the above requirement for small nanodiamonds (radii = 0.5 – 1.5 nm) to explain the mid-infrared emission bands.

7. Nanodiamonds in the interstellar medium

Nanodiamonds are very stable and resilient species: they can survive the passage of supernova-generated shocks. Only in very fast shocks (velocities in excess of 200 km s^{-1}) will they be eroded by thermal sputtering in the more than million degree post-shock gas (Jones et al. 1996, 1997). The need for a very refractory carbonaceous interstellar dust material is indicated by observations which show an almost constant abundance of gas phase carbon over a wide range of molecular hydrogen abundance (Cardelli et al. 1996; Sofia et al. 1997). Thus, indicating little exchange of carbon between the gaseous and solid phases in the interstellar medium. This would be consistent with a large fraction of the solid carbon being in a very refractory phase such as diamond.

7.1. Visible and ultraviolet absorption and emission

Presolar nanodiamonds in the laboratory are a pale grey or brown colour and therefore absorb visible radiation. Then by implication, infrared emission bands arising on nanodiamond surfaces will be excited by visible photons. Such absorption is required to explain the emission bands observed in the reflection nebula *vdB 133* (Uchida et al. 1998), the galaxy *M31* (Cesarsky et al. 1998; Paganì et al. 1999), and elliptical galaxies (Madden et al. 1999), where there is little ultraviolet radiation.

Duley (1988) noted a remarkable similarity in the sharp emission features observed in the luminescence spectra of terrestrial diamonds and those seen in the Red Rectangle. This observation therefore seems to lend further support to the presence of diamonds in the interstellar medium.

Sandford (1996) suggested that the meteoritic diamonds could be the carrier of the 217.5 nm extinction feature. His argument was that complete surface reconstruction to sp^2 carbon will de-localise the π electrons (e.g., Fig. 3) and lead to a surface plasmon mode analogous to that of graphite. Diamond absorbs strongly at ultraviolet wavelengths and therefore nan-

odiamonds should contribute to the ultraviolet extinction (Lewis et al. 1989).

7.2. Observational constraints

In the model proposed here one type of particle, namely surface-reconstructed nanodiamonds, is invoked as the carrier of three different observed interstellar dust properties; the infrared emission bands (a property of the sp^2 carbon surface CC and CH groups), the ultraviolet extinction bump (a property of the sp^2 surface connectivity) and a contribution to the ultraviolet extinction (a property of the overall grain radius and optical properties). The first two properties are related to different surface effects and the third is due to the particle size and absorptivity. These three observable properties of nanodiamond may therefore not be well correlated, even though they arise from the same particles. A lack of correlation between the 217.5 nm extinction bump and the ultraviolet extinction is clearly required by the observational constraints (e.g., Mathis 1990). However, a correlation between the area of the extinction bump and the strength of the infrared emission bands has been observed (Boulanger et al. 1994) which would be consistent with both features arising in the same type of particles.

Recent tight observational constraints on the abundance of carbon in the interstellar medium now place severe limitations on interstellar dust models (e.g., Snow & Witt 1995, 1996). Thus, any dust model that uses one material, in the same dust particles, to explain several of the observed properties of interstellar dust will more easily be able to meet the strict abundance constraints. Interstellar nanodiamonds as an abundant and important grain component, would therefore certainly help to resolve this problem.

8. Summary

We propose that nanodiamonds are an important component of interstellar dust, and that far from being difficult to observe we have in fact long been observing them. We suggest, principally based on laboratory work on the morphological properties of presolar nanodiamonds, that they may be a major contributor to the unidentified interstellar mid-infrared emission bands in the $3 - 15 \mu\text{m}$ region. The emission from nanodiamonds in interstellar and circumstellar media will be driven by the stochastic absorption of visible and ultraviolet photons leading to peak temperatures in the range $\sim 100 - 1000 \text{ K}$.

It seems apparent that this model inherently encompasses aspects of both the PAH (e.g., the specific polyatomic emitting species) and coal model hypotheses (e.g., the three-dimensional nature of the carrier), and may thus provide a bridge between these two research fields.

The nanodiamond hypothesis presented here naturally explains the positions of the emission bands, the dominance of the $11.3 \mu\text{m}$ solo CH feature, the presence of a band at $11.0 \mu\text{m}$, and the relative invariance of the emission spectra and the band-to-band intensity ratios. These are explained by a nanodiamond surface origin for the bands and by the fact that the structural

properties of nanodiamond surfaces are relatively insensitive to the particle size.

In addition to making a major contribution to the mid-infrared emission bands, interstellar nanodiamonds may also be the source of the 217.5 nm extinction bump and may make an important contribution to the ultraviolet extinction.

One interesting and useful outcome of this hypothesis is that it can lead to an easing of the tight constraints placed on interstellar dust models by putting three dust properties into one particle, namely, the infrared emission bands, the 217.5 nm extinction bump and a contribution to the ultraviolet extinction. The fact that these three dust emission and extinction properties do not seem to be well correlated is consistent with the hypothesis. This arises because the three properties arise from different aspects of the particle, namely surface molecular groups, the continuity of the sp² surface and the particle size, respectively.

The infrared band carriers and the VSGs in this hypothesis are one and the same species. The characteristics of each type of particle, derived from the interpretation of observational data, are just different aspects of the emission from one type of particle. The smaller particles, stochastically heated to high temperatures, produce the emission bands, and the cooler larger particles produce underlying plateaux/continua. In high excitation regions the infrared emission band-to-continuum ratio should decrease as the grain core increasingly contributes to the continuum emission. Other bands in the $\approx 4, 5, 10 - 15$ and $21 \mu\text{m}$ regions may also be seen in emission in high excitation regions. It is also likely that the smallest nanodiamond grains, stochastically heated to temperatures of the order of 1000 K, could give rise to an infrared continuum in the $2 - 3 \mu\text{m}$ wavelength region.

Clearly, in order to fully exploit and develop the proposed interstellar nanodiamond hypothesis new experimental and theoretical developments are required. However, both of these fields will be difficult to pursue in the nanometre-size particle regime. The experiments will be hampered by the very active surface chemistry of nanodiamonds, and by the need to isolate and study such small particles. Theoretical developments will rely on modelling particles with of the order of hundreds to thousands of atoms using some form of a quasi-quantum mechanical approach, rather than trying to extrapolate bulk properties to nanometre size scales which is clearly inappropriate.

Acknowledgements. We thank H. Hill, F. Boulanger, L. Verstraete and S. Madden for fruitful discussions on the nature of nanodiamonds and interstellar grains.

References

- Alam M., DebRoy T., Roy R., et al., 1989, *Carbon* 27, 289
- Allamandola L.J., 1989, In: Allamandola L.J., Tielens A.G.G.M. (eds.) *Interstellar Dust*. Kluwer, Dordrecht, p. 129
- Allamandola L.J., Sandford S.A., Tielens A.G.G.M., et al., 1992, *ApJ* 399, 134
- Allamandola L.J., Sandford S.A., Tielens A.G.G.M., et al., 1993, *Sci* 260, 64
- Allamandola L.J., Hudgins D.M., Sandford S.A., 1999, *ApJ* 511, L115
- Anders E., Zinner E., 1993, *Meteoritics* 28, 490
- Andersen A.C., Jorgensen U.G., Nicholaisen F.M., et al., 1998, *A&A* 330, 1080
- Angus J.C., Buck F.A., Groth T.F., et al., 1989, *Materials Research Society Bulletin* 38
- Bachmann P.K., Leers D., Lydtin H., 1991, *Diamond and Related Materials* 1, 1
- Bernatowicz T.J., Gibbons P.C., Lewis R.S., 1989, *Lunar Planet. Sci.* XX, 65
- Bernatowicz T.J., Gibbons P.C., Lewis R.S., 1990, *ApJ* 359, 246
- Blake D.F., Friedmann F., Krisnan K.F.M., et al., 1988, *Nat* 332, 611
- Boulanger F., 1999, In: d'Hendecourt L., Joblin C., Jones A. (eds.) *Solid Interstellar Matter: The ISO Revolution*. EDP Sciences, Les Ulis, p. 19
- Boulanger F., Prévot M.L., Gry C., 1994, *A&A* 284, 956
- Braatz A., Ott U., Henning Th., et al., 1998, *Meteoritics and Planetary Science* 32, A21
- Brooke T.Y., Sellgren K., Smith R.G., 1996, *ApJ* 459, 209
- Cardelli J.A., Meyer D.M., Jura M., et al., 1996, *ApJ* 467, 334
- Cesarsky D., Lequeux L., Pagani L., et al. 1998, *A&A* 337, L35
- Chin R.P., Huang J.Y., Shen Y.R., et al., 1992, *Phys. Rev. B* 45, 1522
- Daulton T.L., Eisenhour D.D., Bernatowicz T.J., et al., 1996, *Geochim. Cosmochim. Acta* 60, 4853
- Davies G., 1977, In: Walker P.I., Throver P.A. (eds.) *Chemistry and Physics of Carbon*. Marcel Dekker Inc., New York 13, p. 1
- Désert F.-X., Boulanger F., Puget J.-L., 1990, *A&A* 237, 215
- Dorschner J., Henning Th., Jäger C., et al., 1996, *Met. & Planet. Soc. Abstracts* 31, A37
- Duley W.W., 1988, *Ap&SS* 150, 387
- Duley W.W., Williams D.A., 1983, *MNRAS* 205, 67P
- Dwek E., Arendt R.G., Fixsen D.J., et al., 1997, *ApJ* 475, 565
- Fedoseev D.V., Bukhovets V.L., Varshavskaya I.G., et al., 1983, *Carbon* 21, 237
- Frenklach M., Kematick R., Huang D., et al., 1989, *J. Appl. Phys.* 66 (1), 395
- Geballe T.R., 1997, In: Pendleton Y.J., Tielens A.G.G.M. (eds.) *From Stardust to Planetesimals*. ASP, San Francisco, p. 119
- Guillois O., Ledoux G., Reynaud C., 1999, *ApJ* 521, L133
- Hill H.G.M., 1998, Ph.D. Thesis, Muséum National d'Histoire Naturelle, Paris
- Hill H.G.M., d'Hendecourt L.B., Perron C., et al., 1997, *Meteoritics and Planetary Science* 32, 713
- Hill H.G.M., Jones A.P., d'Hendecourt L.B., 1998, *A&A* 336, L41
- Jones A.P., Tielens A.G.G.M., Hollenbach D.J., 1996, *ApJ* 469, 740
- Jones A.P., Tielens A.G.G.M., Hollenbach D.J., et al., 1997, In: Bernatowicz T.J., Zinner E. (eds.) *The Astrophysical Implications of the Laboratory Study of Presolar Materials*. AIP, New York, p. 595
- Kapitonov I.N., Kon'kov O.I., 1998, *Astronomy Letters* 24, 468
- Koike C., Wickramasinghe N.C., Kano N., et al., 1995, *MNRAS* 277, 986
- Kuznetsov V.L., Chuvilin A.L., Butenko Y.V., et al., 1994, *Chem. Phys. Lett.* 222, 343
- Lambert D.L., Gustafsson B., Eriksson K., et al., 1986, *ApJS* 62, 373
- Lambrecht W.R.L., Lee C.H., Segall B., et al., 1993, *Nat* 364, 607
- Léger A., Puget J.L., 1984, *A&A* 137, L5
- Lewis R.S., Tang M., Wacker J.F., et al., 1987, *Nat* 326, 160
- Lewis R.S., Anders E., Draine B.T., 1989, *Nat* 339, 117
- Lide D.R., 1992, In: *CRC Handbook of Chemistry and Physics*. CRC Press, Boca Raton, USA, p. 5
- Madden S.C., Vigroux L., Sauvage M., et al., 1999, In: Cox P., Kessler M. (eds.) *The proceedings of the conference: The Universe as seen by ISO*. ESA Special Publications series (SP-427), p. 933

- Mathis J.S., 1990, *ARA&A* 28, 37
- Meilunas R.J., Chang R.P.H., Liu S., et al., 1991, *Appl. Phys. Lett.* 11, 116
- Mitsuda Y., Yamada T., Chuang T.J., et al., 1991, *Surf. Sci. Lett.* 257, L633
- Morelli D.T., Perry T.A., Farmer J.W., 1993, *Phys. Rev. B* 47, 131
- Mutschke H., Dorschner J., Henning T., et al. 1995, *ApJ* 454, L157
- Nuth J.A., Allen J.E., 1992, *Ap&SS* 196, 117
- Ozima M., Mochizuki K., 1993, *Meteoritics* 28, 416
- Papoular R., Conard J., Giuliano M., et al., 1989, *A&A* 217, 208
- Pagani L., Lequeux L., Cesarsky D., et al., 1999, *A&A* 351, 447
- Puget J.L., Léger A., d'Hendecourt L., 1995, *A&A* 293, 559
- Roberts R.A., Walker J., 1967, *Phys. Rev.* 161, 730
- Robertson J., 1986, *Advances in Physics* 35, 317
- Rouleau F., Martin P.G., 1991, *ApJ* 377, 526
- Russell S.S., Arden J.W., Pillinger C.T., 1996, *Meteorit. Planet. Sci.* 31, 343
- Sandford S.A., 1996, *Meteorit. Planet. Sci.* 31, 449
- Saslaw W.C., Gaustad J.E., 1969, *Nat* 221, 160
- Snow T.P., Witt A.N., 1995, *Sci* 270, 1455
- Snow T.P., Witt A.N., 1996, *ApJ* 468, L65
- Sofia U.J., Cardelli J.A., Guerin K.P., et al., 1997, *ApJ* 482, L105
- Tielens A.G.G.M., Seab G.C., Hollenbach D.J., et al., 1987, *ApJ* 319, L109
- Uchida K.I., Sellgren K., Werner M., 1998, *ApJ* 493, L109
- Vanderbilt D., Louie S.G., 1984, *Phys. Rev. B* 30, 6118
- Verstraete L., Puget J.L., Falgarone E., et al., 1996, *A&A* 315, L337